BBA - Proteins and Proteomics 1870 (2022) 140827

Contents lists available at ScienceDirect

BBA - Proteins and Proteomics

journal homepage: www.elsevier.com/locate/bbapap

Antibody binding increases the flexibility of the prion protein

Ioana M. Ilie *, Amedeo Caflisch *

Department of Biochemistry, University of Zurich, Winterthurerstrasse 190, Zurich 8057, Switzerland

A B S T R A C T

Prion diseases are associated with the conversion of the cellular prion protein (PrP) into a pathogenic conformer (PrP^{Sc}). A proposed therapeutic approach to avoid the pathogenic transformation is to develop antibodies that bind to PrP and stabilize its structure. POM1 and POM6 are two monoclonal antibodies that bind the globular domain of PrP and have different biological responses, *i.e.,* trigger neurotoxicity mimicking prion infections (POM1) or prevent neurotoxicity (POM6). The crystal structures of PrP in complex with the two antibodies show similar epitopes which seems inconsistent with the opposite phenotypes. Here, we investigate the influence of the POM1 and POM6 antibodies on the flexibility of the mouse PrP by molecular dynamics simulations. The simulations reveal that the POM6/PrP interface is less stable than the POM1/PrP interface, ascribable to localized polar mismatches at the interface, despite the former complex having a larger epitope than the latter. In the presence of any of the two antibodies, the flexibility of the globular domain increases everywhere except for the β_1-α_1 loop in the POM1/PrP complex which suggests the involvement of this loop in the pathological conversion. The secondary structure of PrP is preserved whereas the polar interactions involving residues Glu146, Arg156 and Arg208 are modified upon antibody binding.

1. Introduction

Prion diseases are transmissible neurodegenerative disorders known as Creutzfeldt-Jakob disease of Gerstman-Straussler-Scheinker syndrome in humans and mad cow disease in bovines. The onset of prion disorders is associated with the conversion of the monomeric form of the prion protein (PrP) into its self-assembled multimeric conformation PrP^{Sc} (scrapie) [1]. The latter propagates by recruiting the non-pathogenic PrP, imposing its conformation upon it and ultimately aggregating into insoluble deposits known as amyloid fibrils, which are identified in the diseased tissue [2]. Structurally, the monomeric form of PrP consists of an unstructured N-terminal segment or flexible tail (residues 23–123) and a globular, folded domain (124–231) [3]. The globular domain is composed of three α-helices α_1 (residues 144–156), α_2 (172–193) and α_3 (200–226), and a two stranded anti-parallel β-sheet (residues 129–132 and 161–163 for β_1 and β_2, respectively) [4] (Fig. 1a). The pathogenic conformer is rich in β-sheets, insoluble and highly resistant to proteolysis [5].

Up to date no treatment has been developed to prevent the development or progression of prion diseases. β-breakers and small molecules were shown to interfere with PrP^{Sc} aggregation and various antibodies increased survival rates [6]. A proposed therapeutic approach is the design of monoclonal antibodies that bind to the monomeric form of PrP and stabilize its native conformation, thereby preventing any conformational changes into the toxic conformer. The POM-family of monoclonal antibodies (POMologues) has been developed to recognize a variety of epitopes along the sequence of PrP [7]. One of such antibodies is POM1, which binds with nanomolar affinity to the globular domain of PrP [8]. When expressed in mice and cerebellar organotypic cultured slices it induces rapid neurodegeneration without distorting the conformation of the globular domain [8] (Fig. 1b). It has been proposed that POM1 acts as a PrP^{Sc} mimetic reagent whose toxicity is mediated by the flexible tail [8,9]. At the opposite pole, POM6 recognizes epitopes neighboring those of POM1, yet it was shown to be innocuous to cerebellar slices [8]. The mechanism of POM1 induced toxicity and its relation to PrP^{Sc} is largely unknown. Moreover, there is no explanation for the distinct biological response of POM6 despite binding to a similar epitope as POM1.

Molecular dynamics (MD) simulations complement experimental studies and provide information on the structural details of free PrP, mutations thereof and PrP in complex with antibodies. Due to its implications and correlation to prion disease susceptibility [10], a lot of attention has been directed towards the conformational behavior of the β_2-α_2 loop (Arg164 – Asn171) [11–15]. In particular, the Val166 – Tyr169 segment was shown to adapt conformation between a 3_{10}-helical turn or a type I β-turn, a conversion regulated by residue Tyr169, which stabilizes the 3_{10}-helical turn [12]. Wild-type PrP has a high free energy barrier to overcome in order to convert the β_2-α_2 segment from a 3_{10}-helical turn to a β-turn [12]. Mutations of the tyrosine decreased the free energy barrier the β_2-α_2 segment needs to overcome to attain the β-turn conformation [12,13]. Furthermore, together with the C-terminal part of the helix α_2, the β_2-α_2 loop was proposed to play an important role in

* Corresponding authors.
E-mail addresses: i.m.ilie@uva.nl (I.M. Ilie), caflisch@bioc.uzh.ch (A. Caflisch).

https://doi.org/10.1016/j.bbapap.2022.140827
Received 10 May 2022; Received in revised form 29 June 2022; Accepted 27 July 2022
Available online 2 August 2022

PrP misfolding in an acidic environment [14]. Another segment of interest is α_1, as the preservation of the helix in its native state was associated with a reduced probability of PrP misfolding [16–19]. Essentially, the detachment of the $\beta_1 - \alpha_1 - \beta_2$ segment from the $\alpha_2 - \alpha_3$ segment results in the exposure of α_1 and its potential misfolding [17,20]. Simulations have shown that pathological mutations can favor fluctuations that promote α_1 detachment from the native packing interface [16]. Additionally, the free energy barrier PrP needs to overcome in order to misfold is associated with the unbroken packing of α_1 [20]. Up to date, the effects of antibody attachment on the structure and flexibility of the globular domain of PrP have not been explored by MD simulations. One exception is a combined simulation and experimental study which has shown that POM1 and neurotoxic mutations thereof induce the formation of a hydrogen bond between the backbone carbonyl group of His140 and the side chain of Arg208, which can alter the flexibility of the β_2-α_2 and α_2-α_3 loops [21]. In a recent simulation study with a simplified model of the membrane and implicit solvent we have focused on the interactions of the flexible tail of PrP with the membrane surface and the globular domain [22]. The simulations showed that the presence of POM1 or POM6 reduced the distance of the flexible tail from the membrane surface. Furthermore, the interactions between the tail and the globular domain were modulated differently by the two antibodies [22]. We did not address a potential influence of the antibodies on the intrinsic plasticity of the globular domain of PrP, which was kept almost rigid to prevent spurious alterations of its folded structure during the enhanced sampling at high temperature.

Here, we investigate the effects of the binding of the neurotoxic POM1 antibody and the innocuous POM6 antibody on the globular domain of mouse PrP. The present study was motivated by the limited knowledge available from the crystal structures which show similar epitopes, [23,24] and thus raise the following questions. Are the contact interfaces and/or the intrinsic flexibility of the PrP globular domain influenced differently by the two antibodies? Are specific interactions between side chains of the globular domain affected by the antibodies? Is the PrP secondary structure preserved in presence of the antibodies? The simulation results show that the complex with POM6 is structurally less stable than the one with POM1. Furthermore, the presence of POM1 or POM6 enhances the flexibility of the PrP globular domain without perturbing its regular elements of secondary structure.

2. Methods

In the following we address only the 125–225 segment of PrP and sometimes omit the term globular domain to simplify the text. For ease of comparison with previous publications, the numbering of the residues refer to the human sequence of PrP which differs from the mouse sequence by one residue.

2.1. System preparation

The starting configurations for the MD simulations were extracted from the solution NMR structure of mouse PrP (PDB ID: 1XYX), [25] and the X-ray diffraction structures of mouse PrP in the complex with POM1 (PDB ID: 4H88) [8] or POM6(PDB ID:6AQ7). [24] To reduce computational cost, only the globular domain of PrP (residues 125–225, Fig. 1a) and only the variable domains of the antibodies were used (residues 1–120 and 1–117 of heavy chain and 1–109 and 1–113 of light chain for POM1 and POM6, respectively, Fig. 1b-c).

2.2. Simulation protocol

The simulations were carried out using the GROMACS 2020.5 simulation package [26,27]. All simulations were performed using the all-atom CHARMM36m forcefield [28] and the TIP3P water model [29]. Three sets of simulations were carried out (with different initial random velocities) for each system: ten 500-ns simulations of mouse PrP, ten 500-ns simulations of PrP in complex with the variable domains of POM1 or POM6, and five 400-ns simulations of POM1 and POM6. The N- and C-termini of all fragments were capped with acetyl and *N*-methylacetamide groups, respectively. All histidine side chains were modeled as neutral and protonated at N_δ. Each complex was then solvated in a cubic box (edge length of 7 nm for free PrP and 10.5 nm for the complexes) with TIP3P water molecules [29] to which 150 mM NaCl were added, including neutralizing counterions. The volume of the simulation box was chosen such that the minimal distance between of the complex to the wall was 1.0 nm and no interaction between the periodic images was felt. Following the steepest descent minimization, the systems were first equilibrated under constant pressure for 5 ns, with position restraints applied on the heavy atoms of the proteins, followed by a 5 ns NPT equilibration in absence of restraints. The temperature and pressure were maintained constant at 300 K and 1 atm, respectively, by using the modified Berendsen thermostat (0.1 ps coupling) [30] and barostat (2 ps coupling) [31]. The production simulations were performed in the NVT ensemble in absence of restraints. The short-range interactions were cut off beyond a distance of 1.2 nm, and the potential smoothly decays to zero using the Verlet cutoff scheme. Periodic boundary conditions were used and the Particle Mesh Ewald (PME) technique [32] was employed (cubic interpolation order, real space cutoff of 1.2 nm and grid spacing of 0.16 nm) to compute the long-range electrostatic interactions. Bond lengths were constrained by means of a fourth order LINCS algorithm

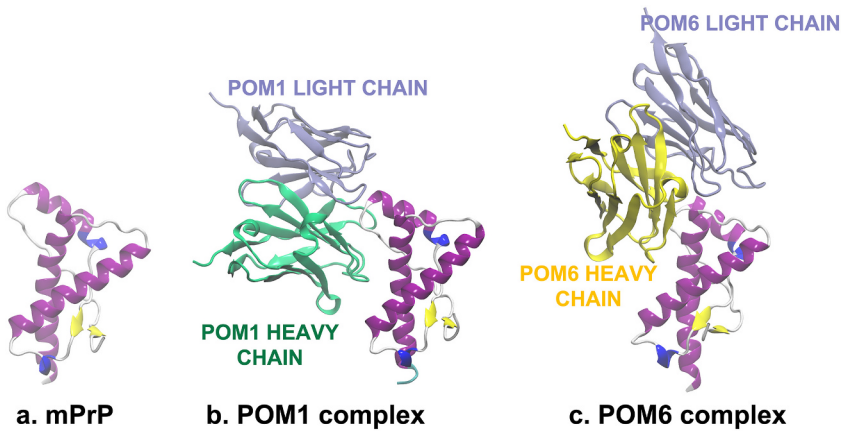

Fig. 1. Simulation systems. (a) Solution NMR structure of the mouse PrP globular domain, and the crystal structures of mouse PrP in complex with the variable domains of (b) POM1 and (c) POM6. The PrP globular domain includes a two-stranded β-sheet (residues 129–132 and 161–163 for strands 1 and 2, respectively), helix α_1 (residues 144–156), helix α_2 (residues 172–193), and helix α_3 (residues 200–22).

with 2 iterations [33]. In all simulations the time-step was fixed to 2 fs and the snapshots were saved every 25 ps.

2.3. SAPPHIRE analysis

The SAPPHIRE (States and Pathways Projected with High Resolution) plot [34,35] displays the states sampled by a complex system and the order in which they are visited along one or multiple trajectories. In this plot, the snapshots are rearranged and grouped according to geometric similarity as defined by a metric given as input. Starting from a random snapshot, the remaining snapshots are ordered by allowing the frame similar to any prior entry in the sequence to become the next item in the array of data. The data is thereby partitioned into basins consisting of similar snapshots without any *a priori* clustering or overlap between the distinct states. The resulting sequence of snapshots is referred to as the progress index. The progress index is annotated with suitable variables, which highlight the conformationally and/or kinetically homogeneous states and the dynamics between them. Here, we define the metric as the RMSD of interatomic distances, which have been identified to play an important role in the stabilization of the globular domain of PrP (Fig. S4). These distances have been selected from an analysis of the literature and by visual inspection. We perform the clustering analysis considering the trajectories of all systems except for the runs S5, S6, S9 and S10 during which the interface with POM6 is not stable.

3. Results

3.1. The interface stability is higher for POM1 than POM6

The globular domain of PrP is structurally stable with average deviations from the crystal structures of 0.25 ± 0.02 nm for free and POM1 complexed PrP, and 0.18 ± 0.02 nm for POM6 complexed PrP (Fig. S1). The variable domains of the antibodies are also structurally stable both in complex with PrP (0.15 ± 0.02 nm for POM1 and 0.21 ± 0.06 for POM6) and in absence of PrP (0.15 ± 0.01 nm for POM1 and 0.16 ± 0.02 for POM6, Fig. S2). In contrast, the PrP/antibody interface varies between the two antibodies. In the POM1 complexes the RMSDs of the antibody show small deviations from the crystal structure (Fig. 2a). The RMSDs of POM6 show heterogenous behavior ranging from small deviations from the initial positions (≈ 0.5 nm) to displacements up to 2 nm (Fig. 2b). The latter correspond to rotations of the antibody around the binding site or partial detachments of POM6 from PrP. Despite the fact that POM6 recognizes a larger contact interface than POM1 [24] and has complementary net charge with PrP (−2, −4 and + 10 net charge for PrP and the variable domains of POM1 and POM6, respectively), the simulations suggest that the POM6/PrP bound state is weaker than POM1/PrP. The stable POM1/PrP interface is consistent with the high affinity of POM1 for PrP (single-digit nanomolar [8]). The ability of POM1 to strip PrP from the POM6-coated surface in pair-wise mapping experiments [7] is consistent with the simulation results. Despite the favorable net charge complementarity of POM6 and PrP, localized polar mismatches may contribute to the instability of the interface. The electrostatic repulsion between Glu200 of PrP and Asp100 of the POM6 heavy chain (^{hc}Asp100) disrupts the Glu200–^{hc}Arg49 salt bridge (Fig. S4). In the following, for the comparative analysis of the two antibodies we exclude the four runs of POM6/PrP with RMSD larger than 1.5 nm (runs S5, S6, S9 and S10 in Fig. 2b).

3.2. Antibody binding increases the flexibility of PrP

The analysis focused on the protein flexibility reveals that the presence of the antibodies increases the overall intrinsic plasticity of *PrP* (Fig. 3). The higher fluctuations at the β-sheet are consistent with nuclear magnetic resonance spectroscopy data on the loosening of the β-sheet upon POM1 binding [8]. The most pronounced increase in flexibility is observed for the Arg156-Asn197 segment, with fluctuations almost three times as high when the antibodies are attached compared to the free state of PrP. The increased flexibility of this region is consistent with previous simulation studies of the POM1/PrP complex [21]. The Arg156-Asn197 segment encompasses the β_2-α_2 loop (Arg164 – Asn171), which was previously shown to adopt 3_{10}-helical turn and β-turn conformations [10]. Unlike in previous studies in which mutations in this segment altered the conformations of the loop [11–13], the presence of the antibodies has no significant impact on the secondary structure of the residues in the loop (Fig. S5a). Additionally, the solvent accessible surface of the segment Tyr169-Phe175 is essentially identical for all systems, *i.e.,* 10.6 ± 0.03 nm^2, 10.6 ± 0.02 nm^2 and 10.5 ± 0.06 nm^2 for free PrP and in contact with POM1 and POM6, respectively. Overall, the flexibility of the globular domain of PrP is increased similarly with the only difference at the Met138-Glu152 segment, *i.e.,* POM1 decreases whereas POM6 increases the flexibility of this segment as compared to free PrP.

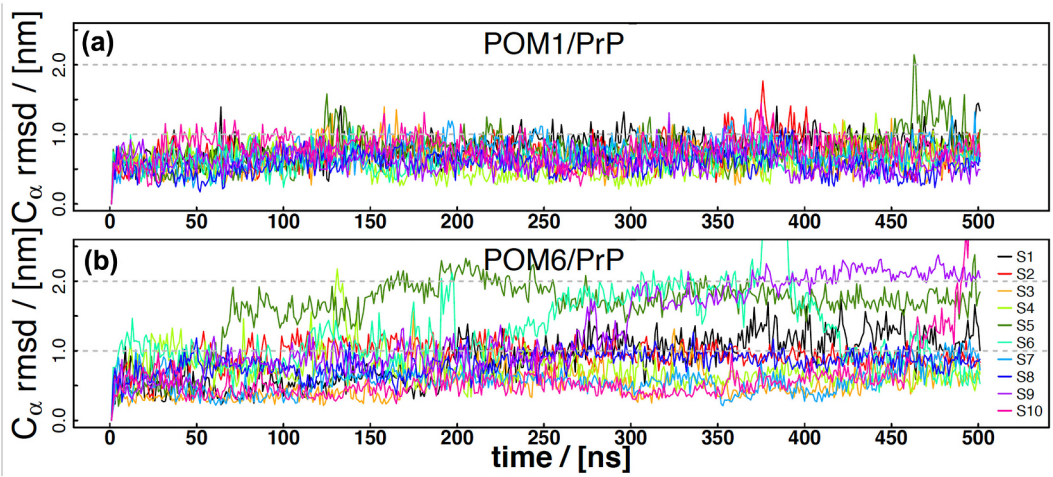

Fig. 2. The complex of PrP with POM6 is less stable than the one with POM1. Shown are the time series of the displacement of the POM1 (a) and POM6 (b) antibody with respect to the globular domain of PrP. The reference crystal structure is the complex with POM1 (PDB code 4H88) [23] or POM6 (PDB code 6AQ7). [24] First the structural alignment of the individual snapshots saved along the MD simulations is carried out on the C_α atoms of the PrP globular domain. Then for each MD snapshot the antibody C_α root-mean-square deviation (RMSD) is calculated as $\sqrt{\frac{1}{N_{ab}}\sum_{i=1}^{N_{ab}}\left(\mathbf{r_i}-\mathbf{r_i^{ref}}\right)^2}$, where $\mathbf{r_i}$ and $\mathbf{r_i^{ref}}$ are the actual and reference coordinates, respectively, of the antibody C_α atom *i*. N_{ab} is the number of residues in the antibody variable domain.

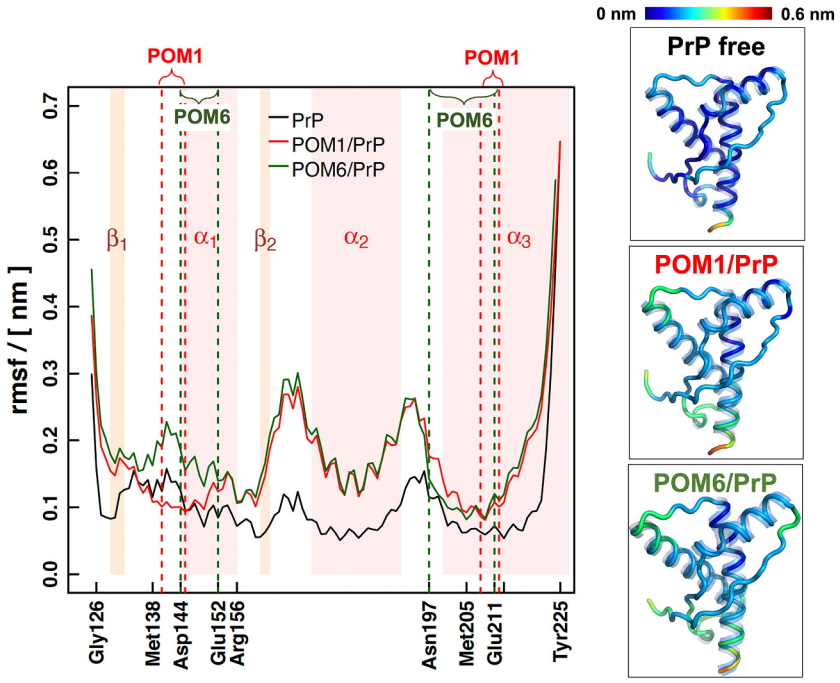

Fig. 3. Root mean square fluctuations (RMSF) profiles of mouse PrP. (left) Compared are the free PrP (black), PrP in the POM1/PrP complex (red) and PrP in the POM6/PrP complex (green). The RMSF profiles are calculated as the average over 50 independent 100-ns profiles. For the POM6 simulations only 30 independent 100-ns profiles are used from the systems with a stable interface (rmsd below 1.5 nm). The discontinuous epitopes of PrP are highlighted (red and green vertical dashed lines for POM1 [23] and POM6 [24], respectively). (right) Fluctuations mapped onto the ribbon representation on PrP. The flexibility is highlighted by the coloring of the ribbons, *i.e.,* from blue to red. (For interpretation of the references to colour in this figure legend, the reader is referred to the web version of this article.)

3.3. *Antibody binding alters two networks of polar contacts in PrP*

The overall increase in flexibility of the globular domain of PrP upon antibody binding correlates with the modifications in PrP intramolecular contacts. For instance, the network of polar interactions involving residues Lys204, Glu146, Asn143 and Arg208 is altered upon antibody attachment (Fig. 4). In the free state, the side chain of Glu146 forms a favorable hydrogen bond with Asn143 (about 50% of the simulation time, Figs. 4b). The presence of POM1 promotes the formation of the Lys204-Glu146 and Glu146-Asn143 salt bridge and hydrogen bond, respectively, (Fig. 4a-c). Essentially, ^{lc}Trp94 from the POM1 light-chain contacts Glu146 (residue in helix α_2), pushing it closer to Asn143 (residue in the $\beta_1 - \alpha_1$-loop) and allowing it to form more frequent hydrogen bonds with Lys204 (residue in helix α_3) (Fig. 4e). The

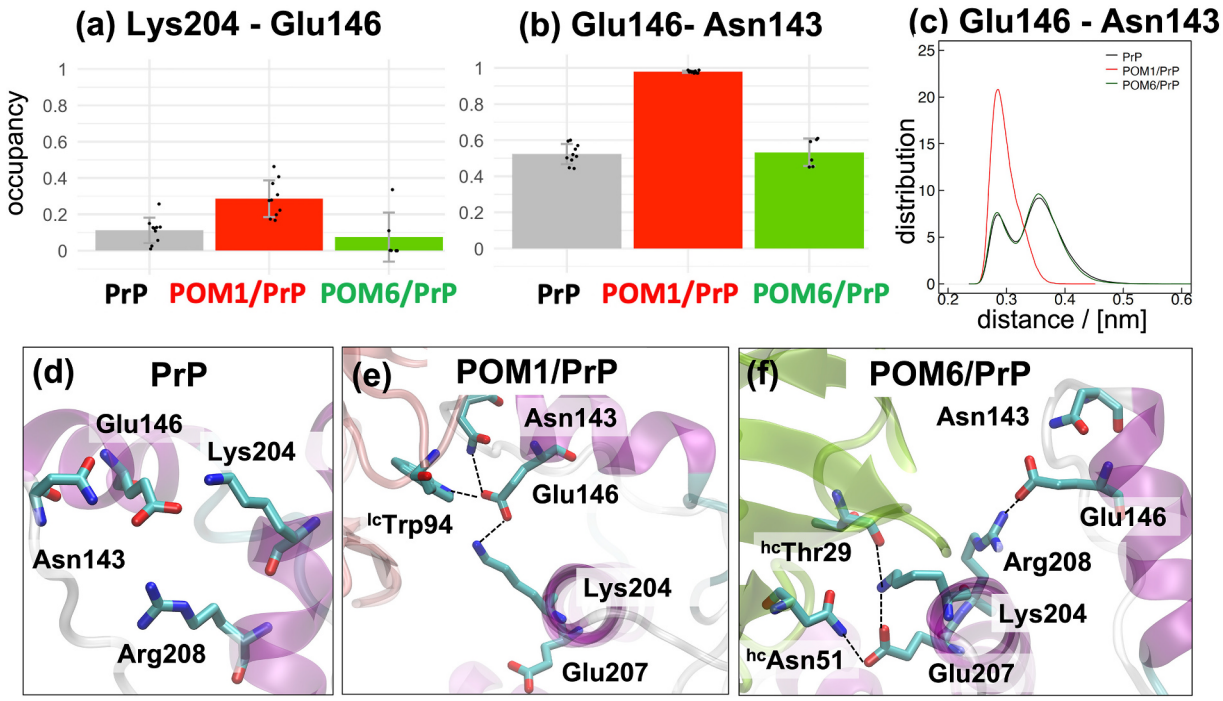

Fig. 4. Polar interactions of PrP residue Glu146. (a), (b) Occupancy of a specific contact averaged per simulation system. Two residues are considered to be in contact if the distance between any of their non-hydrogen side chain atoms is below 0.35 nm. The error bars represent the standard error of the mean calculated as the standard deviation of the average values over the independent runs (black points). (c) Distribution of the Glu146-Asn143 distance cumulated over all simulations. (d-f) Different contacts between the residues in the three analyzed systems. PrP is colored by the secondary structure assignment, POM1 and POM6 by pink and green ribbons, respectively. (For interpretation of the references to colour in this figure legend, the reader is referred to the web version of this article.)

combined effect of these contacts reduces the plasticity of the Met138-Glu152 segment. In contrast, upon POM6 binding, Lys204 is pushed away from Glu146 by residues ^{hc}Asn51 and ^{hc}Thr29 in the POM6 heavy chain (Fig. 4f). Interestingly, the attachment of POM6 has only a marginal effect on the Lys204-Glu146-Asn143 network of contacts and distance distributions (Fig. 4a-c), suggesting that the increased flexibility of the Met138-Glu152 segment has a different source.

In this sense, we identify Arg208 as a key residue, which contributes to the flexibility of the Met138-Glu152 segment. In the free state, the Arg208 side chain can form salt bridges with Glu146, Glu211 or hydrogen bonds with the backbone oxygen of His140 (Fig. 5a,b). In the POM1/PrP complex, the Arg208-His140-Glu146 pocket is located at the POM1 epitope (Fig. 5c), which promotes the formation of the Glu146–^{lc}Trp94 contact. As a consequence, the occupancy of the Arg208-Glu146 salt-bridge is significantly reduced as compared to free PrP (Fig. 5a top). Additionally, due to the presence of the antibody, the conformational space of His140 is reduced, which in turn promotes the formation of the Arg208-His140 hydrogen bond (Fig. 5a,c) and subsequently leads to a more rigid Met138-Glu152 segment. In the POM6/PrP complex, only part of the pocket is located at the POM6 epitope and Glu146 contacts ^{hc}Gln99 of the antibody heavy chain (Fig. 5d). The occupancy of the Arg208-Glu146 salt bridge is reduced, while the population of the Arg208-His140 hydrogen bond and Arg208-Glu211 salt-bridge is comparable to free PrP. The net effect of these interactions is to break the contact between helices α_3 and α_1 and thereby contributes to the increased flexibility of the Met138-Glu152 segment upon POM6 attachment.

The increased flexibility of the β_2-α_3 segment in presence of both antibodies is correlated with the contacts involving Arg156. The attachment of the antibodies stimulates the formation of the Arg156-Asp202 salt-bridge and the Arg156-Asn153 hydrogen bond, and reduces the Arg156-Glu196 salt bridge (Fig. 6a). In the free state the Arg156-Asp202-Asn153 pocket is solvent exposed enabling the arginine side chain to be involved either in contacts with its immediate pocket neighbors (Fig. 6b) or to rotate and bind to Glu196 *via* a salt bridge (Fig. 6c). The latter connects the α_1-β_2 loop to the α_2-α_3 loop and thereby contributes to the reduced flexibility of the β_2-α_3 segment in free PrP (Fig. 3). In the POM1/PrP complex, the Arg156-Asp202-Asn153 pocket remains solvent exposed, which reflects on the comparable occupancy of the Arg156-Glu196 salt-bridge. In the POM6/PrP complex, the Arg156-Asp202-Asn153 pocket is part of the POM6 epitope. Thereby, the insertion of ^{lc}Ser32 of the POM6 light chain reduces the formation of the Arg156-Glu196 salt bridge and promotes more frequent contacts within the Arg156-Asp202-Asn153 pocket (Fig. 6a,d). The complex interplay of these interactions reflects on the RMSF profile of the β_2-α_3 segment.

3.4. SAPPHIRE analysis of the conformational space of PrP

We annotate the SAPPHIRE plot with the interatomic distances discussed throughout this manuscript and additional intramolecular distances previously highlighted to discriminate between the complexes with POM1 or POM6. The barriers on the cut function (*i.e.,* the local

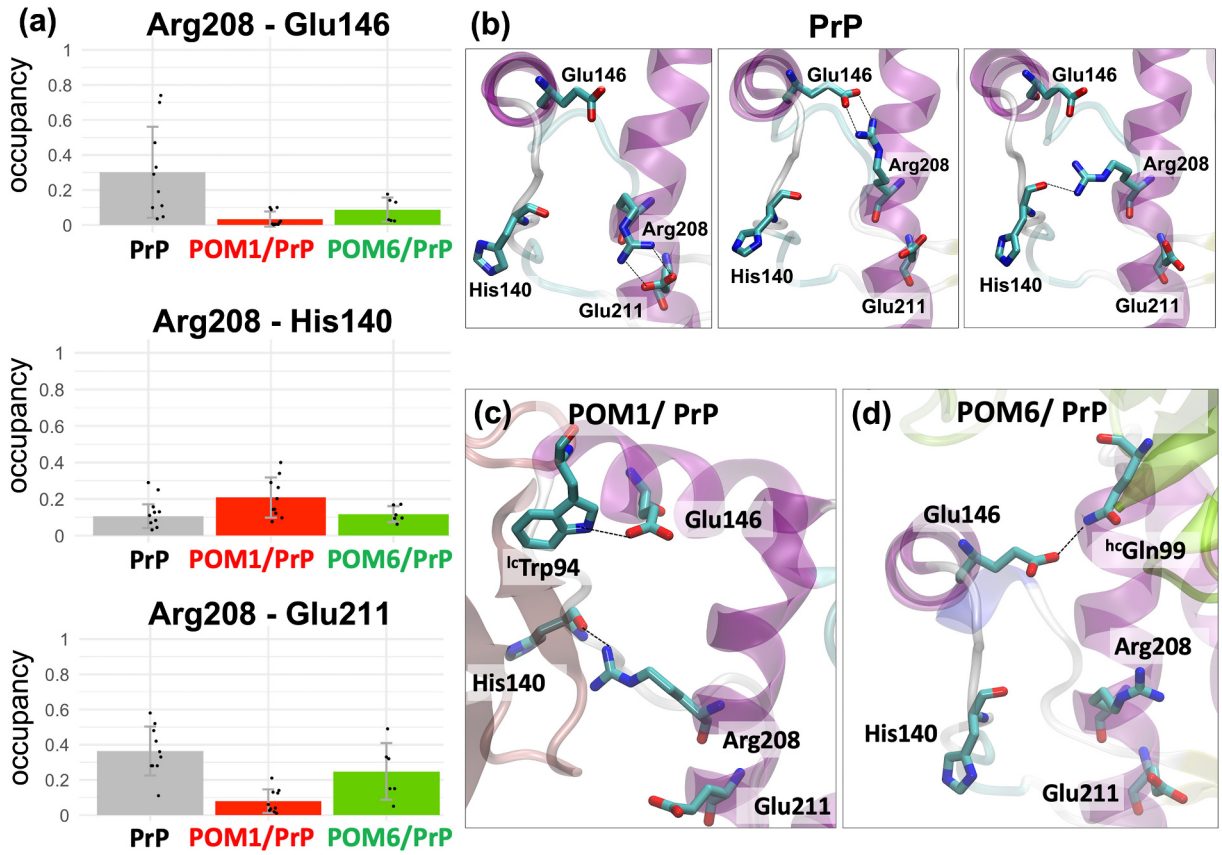

Fig. 5. Polar interactions of PrP residue Arg208. (a) Occupancy of a specific contact averaged per simulation system. Two residues are considered to be in contact if the distance between any of their non-hydrogen side chain atoms is below 0.35 nm. For the occupancy of the Arg208-His140 hydrogen bond a contact is considered when the distance between the backbone oxygen atom of His140 and the Cz of Arg208 is below 0.4 nm. The error bars represents the standard error of the mean calculated as the standard deviation of the average values over the independent runs (black points). (b) Different contacts Arg208 can form in free PrP. (c) Snapshot of the Arg208-His140 hydrogen bond in the POM1/PrP complex. To facilitate the visualization, the prion protein is rotated by 90 degrees. (d) Snapshot of the network of contacts in the POM6/PrP complex. PrP is colored by the secondary structure assignment, POM1 and POM6 by pink and green ribbons, respectively. (For interpretation of the references to colour in this figure legend, the reader is referred to the web version of this article.)

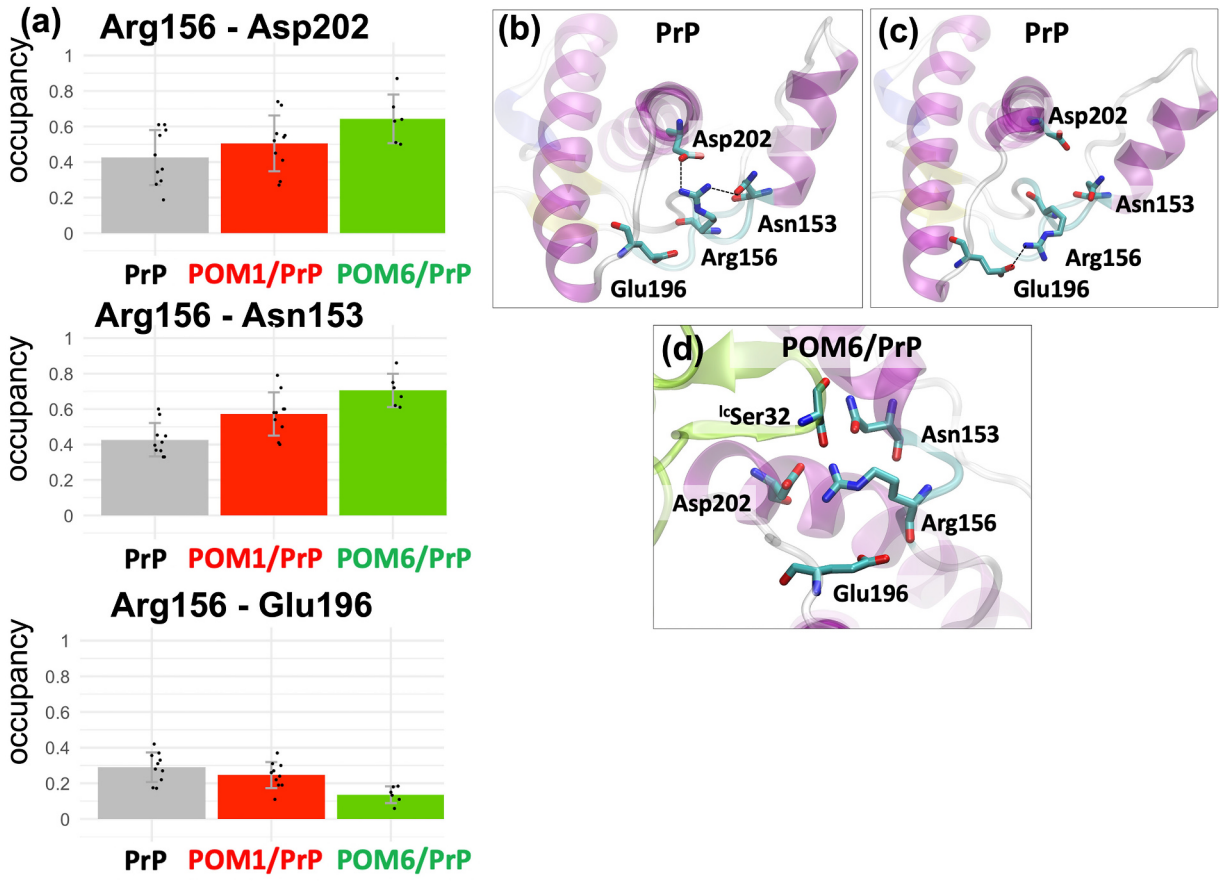

Fig. 6. Polar interactions of PrP residues Arg156. Same as Fig. 4 for residue Arg156.

maxima on the profile in black in the bottom part of Fig. 7) separate individual metastable states. The statistical weight of each state can be quantified as the progress-index segment between two consecutive barriers. Importantly, recurrence across the individual simulations and systems shows that most basins are sampled several times and in different simulation systems (black, red and green dots in the middle part of Fig. 7). The first 8×10^4 snapshots along the progress index are grouped into a single basin, which includes states sampled predominantly by PrP in complex with the antibodies and less by free PrP (Fig. 7 top left for a representative snapshot). In contrast, the following small basin (between 8×10^4 and 9×10^4) highlights states that are rarely identified in the POM1 complex and are characterized by the presence of the Arg208-Glu146 contact (see Fig. 5b-middle for a representative snapshot). The structural annotation highlights the consistency with the contact analysis involving residues Arg156 in Fig. 6 and Arg208 in Fig. 5. The basins between 3×10^5 and 4×10^5 highlight states that are populated mainly by the free PrP and PrP in complex with POM6. The states are characterized by close contacts in the Arg156-Asp202-Asn153-Tyr149 pocket, which stabilize the interaction between α_1 and α_3 (Fig. 7 middle snapshot). The remaining basins are populated by all three analyzed systems. We highlight the basin between 4.2×10^5 and 4.7×10^5, which is populated with predominance by PrP in complex with POM1 (higher density of red dots). This basin is characterized by the formation of the Arg208-His140 hydrogen bond and the formation of the Lys204-Glu146 salt bridge, both of which push the β_1 - α_1 loop closer to α_3 and may contribute to the reduced flexibility of the Met138-Asp144 segment in the presence of POM1 (Fig. 7 snapshot right and Fig. 3).

3.5. *Antibody binding increases the 3_{10}-helix occupancy of the C-terminal turn of helix α_1*

The importance of the $\beta_2 - \alpha_2$ loop and its association with toxicity has been repeatedly underlined [10] and investigated for free PrP and single point mutations in its globular domain [11–14]. Despite the substantially higher fluctuations in the $\beta_2 - \alpha_2$ loop (Fig. 3), antibody binding has no effect on the secondary structure of the loop with the 3_{10}-helix remaining the most populated conformation (≈ 90% of the simulation time, Fig. S5). The higher fluctuations are a consequence of rigid body motion (see Movie S1) which do not perturb the 3_{10}-helix conformation. On the other hand, antibody attachment affects the conformations of the C-terminal turn of helix α_1, whose structural preservation is essential to avoid PrP misfolding [16,17,20]. In the free state, the Met154-Arg156 segment adopts mainly β-turn conformations (≈ 60% of the simulation time); it can occasionally transform into a 3_{10}-helix (≈ 30% of the simulation time) and is only rarely involved in a bend (Fig. 8 and Fig. S5). The presence of POM1 does not alter the β-turn occupancy of the Met154-Arg156 segment, which populates more abundantly the 3_{10}-helical conformation. The presence of POM6 further increases the occupancy of the 3_{10}-helical state up to 60% and reduces the population of β-turns by about 20%.

4. Discussion

The POM-family of antibodies has been designed to recognize different epitopes along the sequence of PrP and modulate prion induced toxicity [7]. Two of the developed monoclonal antibodies recognize similar epitopes on the surface of the globular domain and have different biological response, *i.e.,* POM1 is neurotoxic and POM6 is innocuous [7]. The crystal structures of PrP in complex with these antibodies have been

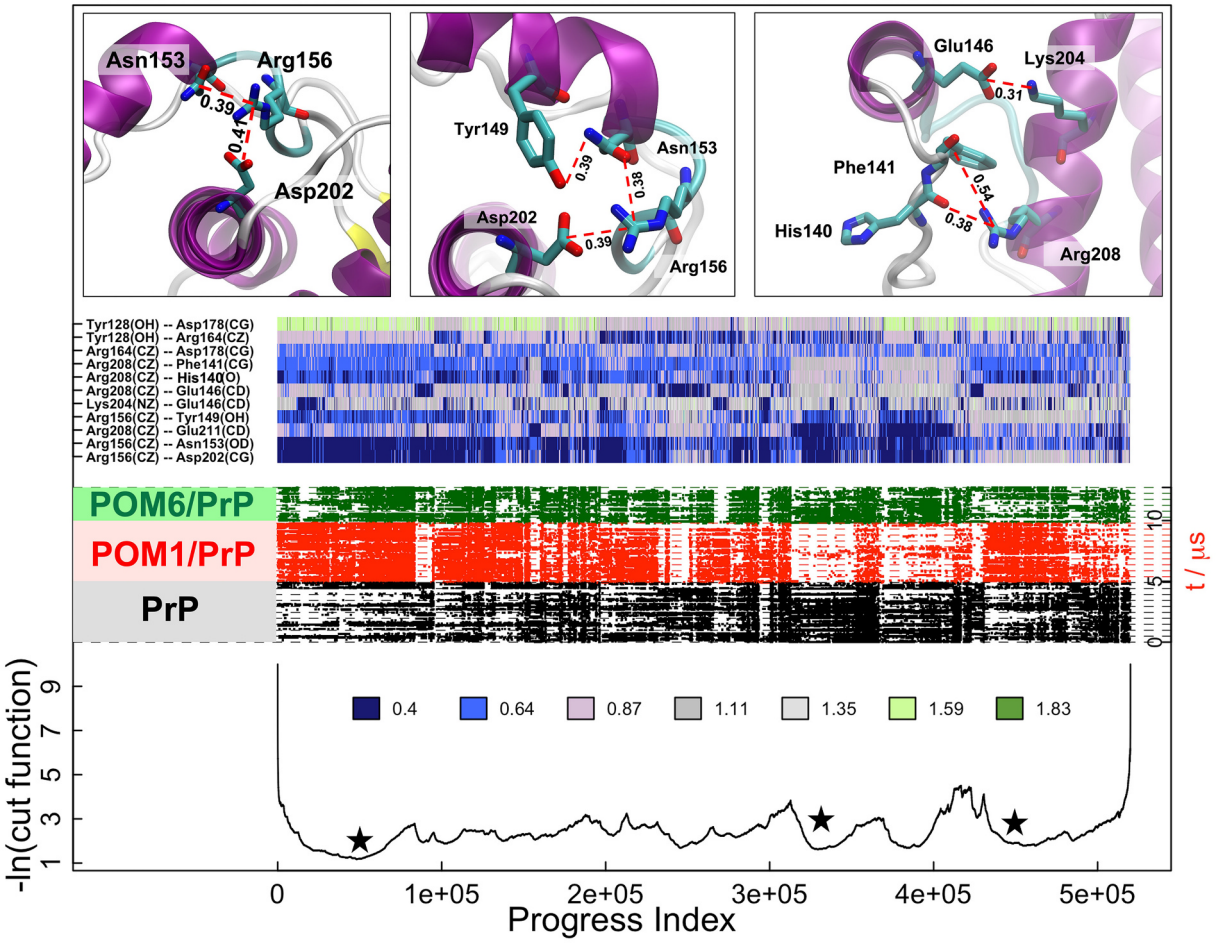

Fig. 7. SAPPHIRE plot of the conformational space of PrP. (Bottom) The progress index corresponds to the reordering of the snapshots according to pairwise structural similarity. The cut function (black line) is constructed by counting transitions along the simulations such that its local minima and maxima correspond to states that are highly populated and barriers that are visited sporadically, respectively. The dynamic trace (black, red, and green dots) localizes the time development of the simulated system along the progress index and cut function. In other words, the dynamic trace reflects the sequence of events as it illustrates the visits to individual states and crossing of barriers for each simulation run where individual runs are separated by horizontal dotted lines. (Middle) PrP intramolecular distances discussed in this manuscript and intramolecular distances previously identified to contribute to the intrinsic plasticity of PrP. The complete list of distances used for the progress index metric is in Fig. S4. The values of the distances are grouped into seven bins (colour legend on top of cut profile). (Top) Representative snapshots extracted from the highlighted basins along the cut profile (stars). (For interpretation of the references to colour in this figure legend, the reader is referred to the web version of this article.)

resolved [23,24], yet little is known on their effects on the structural dynamics of PrP and correlations to toxicity. Here, we investigated the effects of POM1 and POM6 binding on PrP by molecular dynamics simulations. A number of similarities and differences arise from a comparison with previous simulation studies.

First, we report on the increased plasticity of the $\beta_2 - \alpha_2$ loop upon antibody attachment. This is consistent with previous simulations of POM1 in complex with PrP using the same initial conformation [21]. Effects of single point mutations on the plasticity of PrP and the conformational polymorphism of the $\beta_2 - \alpha_2$ loop in context of cytotoxicity have been previously investigated. In particular, the $\beta_2 - \alpha_2$ loop can adopt a 3_{10}-helical conformation or a β-turn. The first is characterized by the inward conformation and thereby reduced solvent exposure of Tyr169 and the latter by the outward conformation of Tyr169, which was proposed to increase the propensity of PrP to transform into PrP^{Sc} [36]. Simulations showed that wild-type mouse PrP needs to overcome a high free energy barrier to transform the $\beta_2 - \alpha_2$ loop from the protective 3_{10}-helical turn to a β-turn [12]. Additionally, single point mutations in this segment were shown to decrease the free energy barrier leading to an increased population of the β-turn conformation [12,13]. The present study shows that the $\beta_2 - \alpha_2$ loop populates mainly a 3_{10}-helical conformation ($\approx$ 90% of the simulation time, Fig. S5) independently of antibody binding.

Second, our results inform on the modified network of intramolecular contacts in PrP upon antibody binding as compared to the free state. A recent experimental and computational study proposed that the attachment of the POM1 antibody induces the formation of a stable hydrogen bond between residues His140 and Arg208 (called H-latch), which controls the toxicity of PrP [21]. Our study confirms that the presence of POM1 promotes the formation of the His140-Arg208 hydrogen bond, yet with less prevalence than previously shown [21]. This discrepancy may arise because of the different protonation states of the His140 side chain in the two studies and/or the use of different force fields. Additionally, we show that upon POM6 binding the hydrogen bond occupancy remains identical to the free state. Our results are consistent with the findings of Frontzek et al. [21], which showed that POM1 binding breaks the Arg156-Glu196 interaction and induces the formation of a Arg156-Asp202 salt bridge thereby increasing the $\alpha_2 - \alpha_3$ flexibility. Additionally, we find that the attachment of the innocuous POM6 antibody has an even higher impact on these contacts, *i.e.,* the Arg156-Glu196 bond is about 50% less populated and the Arg156-Asp202 salt bridge is more abundant than in the presence of POM1.

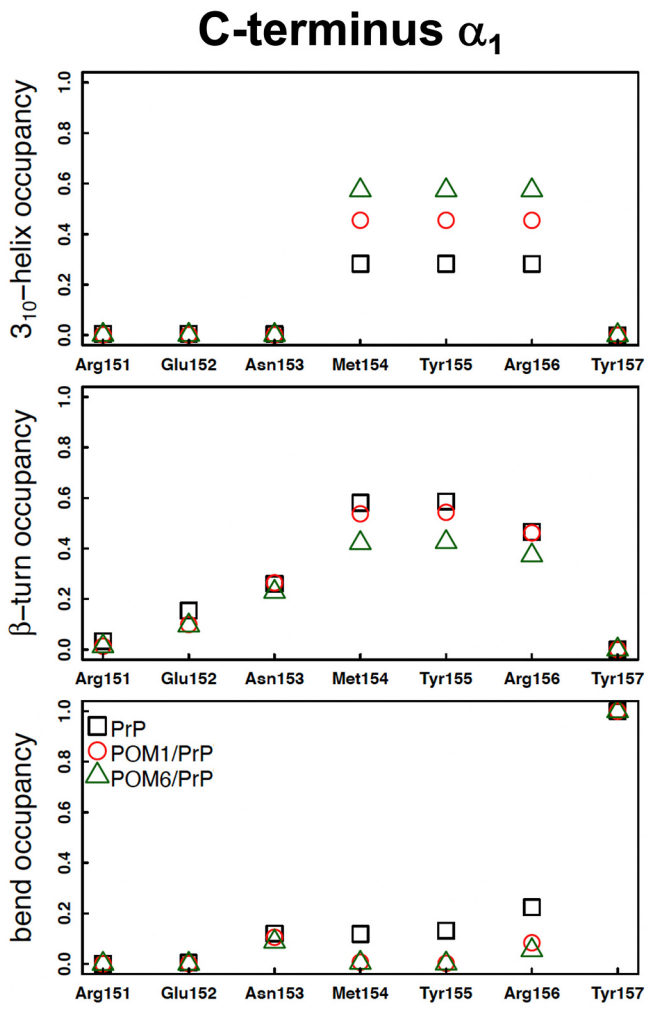

Fig. 8. The antibodies stabilize the C-terminal turn of helix α_1. The propensity for 3_{10}-helix (top), β-turn (middle), and bend (bottom) was calculated by CAMPARI version 4 (http://campari.sourceforge.net/V4/http://campari.sourceforge.net).

Thus, it is not possible to explain the toxic effect of POM1 by monitoring a small set of polar interactions within the globular domain of PrP. Our simulation results provide evidence on the combined effects of the network of intramolecular contacts on the plasticity of PrP.

Third, we reveal that antibody binding increases the propensity of the 3_{10}-helical conformation in the C-terminal turn of helix α_1, with POM6 having a higher impact than POM1. Additionally, POM6 reduces the occupancy of the β-turn in this segment, while POM1 has only marginal effect. Previous studies have shown that the loss of native structure in helix α_1 leads to its detachment from the packing interface, which in turn may increase the probability of PrP misfolding [16,17,19,20]. In this context, the attachment of the antibodies stabilizes the native 3_{10}-helix, but additionally POM6 reduces the propensity of β-turns, which may contribute to preventing the misfolding of PrP.

5. Biological significance

One of the most discussed hypothesis links prion pathogenesis to the gain of toxicity upon PrP conversion to PrP^{Sc} rather than the loss of its physiological function [8,37,38]. This is consistent with the fact that inactivation of the PrP gene in mice or cows does not cause neurodegeneration [37]. Toxicity was proposed to originate from PrP^{Sc} -induced aggregation of PrP on the cell surface, which would generate a neurotoxic signal [38,39]. In this context, PrP^{Sc} may block specific regions or PrP and alter its signaling properties [38]. POM1 binding was proposed to emulate PrP^{Sc} induced toxicity, thereby contributing to the misfolding of PrP [8,40]. Furthermore, experimental evidence suggests that the flexible tail plays a mediating role in PrP^{Sc} -docking (or POM1) associated toxicity [8,41,42].

Prion diseases take years to progress and the mechanisms associated with toxicity, such as structural conversions in the globular domain, exceed the temporal resolution of explicit solvent simulations. Our results provide insight into the early response of PrP to POM1 and POM6 binding, which contribute to the interpretation of experimental observation. For instance, pair-wise mapping experiments revealed that POM1 can strip PrP from the POM6-coated surface [7]. We showed that the weaker POM6/PrP interface is ascribable to localized polar mismatches at the complex interface. Furthermore, nuclear magnetic resonance spectroscopy data reported on the increased flexibility of the structured segments of PrP upon POM1 binding, yet without distorting the overall structure of PrP [8,43]. Here, we observed that the increased flexibility of PrP upon antibody binding correlates with the disruption of the native PrP intramolecular contacts involving residues Glu146, Arg156 and Arg208. Our results on the contact analysis do not allow a direct mapping to experimental toxicity, yet they inform on the more frequent formation of the His140-Arg208 hydrogen in the POM1/PrP complex as compared to wild-type or the POM6/PrP complex. This hydrogen bond has been recently suggested to play a relevant role in the toxicity of PrP [21].

Mutations and truncations in the flexible tail were shown to modulate prion induced neurotoxicity and neuroprotection [41]. The intrinsic disorder and the size (around 100 residues) of the flexible tail does not allow one to obtain statistically converged sampling by explicit solvent simulations. In a previous study, we used implicit solvent simulations and enhanced sampling techniques (with restraints on the dihedral angles of the globular domain of PrP and the antibodies) to analyze the behavior of the flexible tail as well as its interactions with a simplified model of the membrane surface [22]. The wild type flexible tail of PrP and six different truncations thereof were investigated. Those simulations provided evidence that the binding of POM1 and POM6 onto membrane-bound PrP reduces the distance of the flexible tail to the membrane surface and restricts the orientational disorder of the globular domain. Furthermore, the interactions between flexible tail and globular domain are affected differently by the two antibodies. In our previous work we characterized the role of the flexible tail (including interstitial truncations thereof) and the binding of the two antibodies to the membrane-bound prion protein. Here, we emphasize the influence of the antibodies on the dynamics and the structure of the globular domain of PrP and investigate the atomistic detail of the network of intramolecular contacts. Taken together, our explicit solvent simulations (this study) and the previous simulations with a simplified model of membrane and solvent [22] provide a comprehensive picture of the influence of POM1 and POM6 on PrP.

In conclusion, our results lay the foundation for the development of small molecules (*e.g.* organic compounds, peptides) that bind to PrP to modulate its dynamics and thereby prevent its toxic transformation. We propose a synergistic combination of atomistic simulations and *in vitro* experiments to optimize the design of the small-molecule modulators. In an experimental setup, the thermodynamics and kinetics of binding could be tested *via* surface plasmon resonance or isothermal titration calorimetry. In the next step, the good binders (low nanomolar binding affinity) would be evaluated in cellular assays by quantifying their activity in rescuing prion-infected cultured organotypic cerebellar slices [44].

6. Conclusions

We have investigated the effects of binding of a neurotoxic (POM1) and innocuous (POM6) antibody to the globular domain of mouse PrP by explicit solvent MD simulations. The analysis of the MD trajectories has

provided four main observations that go beyond the information available in the crystal structures. First, the POM6/PrP interface is less stable on a 5-μs time scale than the POM1/PrP interface, with displacements of the POM6 antibody up to 2 nm with respect to the crystal structure. Second, the flexibility of the antibody-bound globular domain of PrP increases everywhere except for the β_1-α_1 loop in the POM1/PrP complex which is part of its discontinuous epitope. Third, the PrP intramolecular network of contacts is perturbed differently by the binding of the two antibodies. Fourth, both antibodies stabilize the 3_{10}-helix at the C-terminal turn of helix α_1 (with POM6 having a more pronounced effect) and POM6 also reduces the β-turn propensity in this segment of the PrP sequence. The stabilization of the β_1-α_1 loop by the toxic antibody, and not the innocuous one, suggests a potential role of this loop in the conversion to PrP^{Sc}.

Supplementary data to this article can be found online at https://doi.org/10.1016/j.bbapap.2022.140827.

CRediT authorship contribution statement

Ioana M. Ilie: Conceptualization, Methodology, Software, Validation, Formal analysis, Investigation, Data curation, Writing – original draft, Writing – review & editing, Visualization. **Amedeo Caflisch:** Conceptualization, Resources, Supervision, Funding acquisition, Writing - review & editing.

Declaration of Competing Interest

The authors declare that they have no known competing financial interests or personal relationships that could have appeared to influence the work reported in this paper.

Data availability

Data will be made available on request.

Acknowledgement

The computational resources were provided by the Swiss National Supercomputing Centre (CSCS) in Lugano. The research in AC group is supported by an SNF Excellence Grant (310030B-189363).

References

[1] A. Aguzzi, A.M. Calella, Prions: protein aggregation and infectious diseases, Physiol. Rev. 89 (4) (2009) 1105–1152.
[2] H. Kretzschmar, S. Prusiner, L. Stowring, S. DeArmond, Scrapie prion proteins are synthesized in neurons, Am. J. Pathol. 122 (1) (1986) 1.
[3] R. Zahn, A. Liu, T. Lührs, R. Riek, C. von Schroetter, F. López García, M. Billeter, L. Calzolai, G. Wider, K. Wüthrich, Nmr solution structure of the human prion protein, Proc. Nat. Acad. Sci. 97 (1) (2000) 145–150.
[4] R. Riek, S. Hornemann, G. Wider, M. Billeter, R. Glockshuber, K. Wüthrich, Nmr structure of the mouse prion protein domain prp(121?231), Nature 382 (6587) (1996) 180–182.
[5] M. Zweckstetter, J.R. Requena, H. Wille, Elucidating the structure of an infectious protein, PLoS Pathog. 13 (2017) 1–6.
[6] A. Aguzzi, A.K.K. Lakkaraju, K. Frontzek, Toward therapy of human prion diseases, Annu. Rev. Pharmacol. Toxicol. 58 (1) (2018) 331–351.
[7] M. Polymenidou, R. Moos, M. Scott, C. Sigurdson, Y.-Z. Shi, B. Yajima, I. Hafner-Bratkovič, R. Jerala, S. Hornemann, K. Wuthrich, A. Bellon, M. Vey, G. Garen, M.N. G. James, N. Kav, A. Aguzzi, The pom monoclonals: a comprehensive set of antibodies to non-overlapping prion protein epitopes, PLoS One 3 (12) (2008) 1–17.
[8] T. Sonati, R.R. Reimann, J. Falsig, P.K. Baral, T. O'Connor, S. Hornemann, S. Yaganoglu, B. Li, U.S. Herrmann, B. Wieland, M. Swayampakula, M.H. Rahman, D. Das, N. Kav, R. Riek, P.P. Liberski, M.N.G. James, A. Aguzzi, The toxicity of antiprion antibodies is mediated by the flexible tail of the prion protein, Nature 501 (7465) (2013) 102–106.
[9] M. Bardelli, K. Frontzek, L. Simonelli, S. Hornemann, M. Pedotti, F. Mazzola, M. Carta, V. Eckhardt, R. D'Antuono, T. Virgilio, S.F. Gonzalez, A. Aguzzi, L. Varani, A bispecific immunotweezer prevents soluble prp oligomers and abolishes prion toxicity, PLoS Path. 14 (2018) 1–22.
[10] T.D. Kurt, C. Bett, N. Fernández-Borges, S. Joshi-Barr, S. Hornemann, T. Rülicke, J. Castilla, K. Wüthrich, A. Aguzzi, C.J. Sigurdson, Prion transmission prevented by modifying the β2–α2 loop structure of host prpc, J. Neurosci. 34 (3) (2014) 1022–1027.
[11] D. Huang, A. Caflisch, The roles of the conserved tyrosine in the β_2-α_2 loop of the prion protein, Prion 9 (6) (2015) 412–419.
[12] D. Huang, A. Caflisch, Evolutionary conserved tyr169 stabilizes the β2–α2 loop of the prion protein, J. Am. Chem. Soc. 137 (8) (2015) 2948–2957.
[13] E. Caldarulo, A. Barducci, K. Wüthrich, M. Parrinello, Prion protein β2–α2 loop conformational landscape, Proc. Nat. Acad. Sci. 114 (36) (2017) 9617–9622.
[14] S. Zhou, D. Shi, X. Liu, X. Yao, L.-T. Da, H. Liu, ph-induced misfolding mechanism of prion protein: insights from microsecond-accelerated molecular dynamics simulations, ACS Chem. Neurosci. 10 (6) (2019) 2718–2729.
[15] W. Chen, M.W. van der Kamp, V. Daggett, Structural and dynamic properties of the human prion protein, Biophys. J. 106 (5) (2014) 1152–1163.
[16] A. De Simone, A. Zagari, P. Derreumaux, Structural and hydration properties of the partially unfolded states of the prion protein, Biophys. J. 93 (4) (2007) 1284–1292.
[17] F. Eghiaian, T. Daubenfeld, Y. Quenet, M. van Audenhaege, A.-P. Bouin, G. van der Rest, J. Grosclaude, H. Rezaei, Diversity in prion protein oligomerization pathways results from domain expansion as revealed by hydrogen/deuterium exchange and disulfide linkage, Proc. Nat. Acad. Sci. 104 (18) (2007) 7414–7419.
[18] K. Kuwata, Y.O. Kamatari, K. Akasaka, T.L. James, Slow conformational dynamics in the hamster prion protein, Biochem. 43 (15) (2004) 4439–4446.
[19] J.H. Viles, D. Donne, G. Kroon, S.B. Prusiner, F.E. Cohen, H.J. Dyson, P.E. Wright, Local structural plasticity of the prion protein. Analysis of nmr relaxation dynamics, Biochem. 40 (9) (2001) 2743–2753.
[20] C. Camilloni, D. Schaal, K. Schweimer, S. Schwarzinger, A.D. Simone, Energy landscape of the prion protein helix 1 probed by metadynamics and nmr, Biophys. J. 102 (1) (2012) 158–167.
[21] K. Frontzek, M. Bardelli, A. Senatore, A. Henzi, R.R. Reimann, S. Bedir, M. Marino, R. Hussain, S. Jurt, G. Meisl, M. Pedotti, F. Mazzola, G. Siligardi, O. Zerbe, M. Losa, T. Knowles, A. Lakkaraju, C. Zhu, P. Schwarz, S. Hornemann, M.G. Holt, L. Simonelli, L. Varani, A. Aguzzi, A conformational switch controlling the toxicity of the prion protein, bioRxiv (2021).
[22] I.M. Ilie, M. Bacci, A. Vitalis, A. Caflisch, Antibody binding modulates the dynamics of the membrane-bound prion protein, Biophys. J. 121 (2022) 1–13.
[23] P. Baral, B. Wieland, M. Swayampakula, M. Polymenidou, M. Rahman, N. Kav, A. Aguzzi, M. James, Structural studies on the folded domain of the human prion protein bound to the fab fragment of the antibody pom1, Acta Crystallogr D 68 (2012) 1501–1512.
[24] P.K. Baral, M. Swayampakula, A. Aguzzi, M.N.G. James, Structural characterization of pom6 fab and mouse prion protein complex identifies key regions for prions conformational conversion, FEBS J. 285 (9) (2018) 1701–1714.
[25] A.D. Gossert, S. Bonjour, D.A. Lysek, F. Fiorito, K. Wüthrich, Prion protein nmr structures of elk and of mouse/elk hybrids, Proc. Nat. Acad. Sci. 102 (3) (2005) 646–650.
[26] H. Berendsen, D. van der Spoel, R. van Drunen, Gromacs: a message-passing parallel molecular dynamics implementation, Comput. Phys. Commun. 91 (1) (1995) 43–56.
[27] B. Hess, C. Kutzner, D. van der Spoel, E. Lindahl, Gromacs 4: algorithms for highly efficient, load-balanced, and scalable molecular simulation, J. Chem. Theor. Comp. 4 (3) (2008) 435–447.
[28] J. Huang, S. Rauscher, G. Nawrocki, T. Ran, M. Feig, B.L. de Groot, H. Grubmueller, A.D. MacKerell Jr., Charmm36m: an improved force field for folded and intrinsically disordered proteins, Nat. Methods 14 (2016) 71–73.
[29] W.L. Jorgensen, J. Chandrasekhar, J.D. Madura, R.W. Impey, M.L. Klein, Comparison of simple potential functions for simulating liquid water, J. Chem. Phys. 79 (2) (1983) 926–935.
[30] G. Bussi, D. Donadio, M. Parrinello, Canonical sampling through velocity rescaling, J. Chem. Phys. 126 (1) (2007), 014101.
[31] H.J.C. Berendsen, J.P.M. Postma, W.F. van Gunsteren, A. DiNola, J.R. Haak, Molecular dynamics with coupling to an external bath, J. Chem. Phys. 81 (8) (1984) 3684–3690.
[32] T. Darden, D. York, L. Pedersen, Particle mesh ewald: an nlog(n) method for ewald sums in large systems, J. Chem. Phys. 98 (12) (1993) 10089–10092.
[33] B. Hess, H. Bekker, H.J.C. Berendsen, J.G.E.M. Fraaije, Lincs: a linear constraint solver for molecular simulations, J. Comp. Chem. 18 (12) (1997) 1463–1472.
[34] N. Blochliger, A. Vitalis, A. Caflisch, A scalable algorithm to order and annotate continuous observations reveals the metastable states visited by dynamical systems, Comput. Phys. Commun. 184 (11) (2013) 2446–2453.
[35] F. Cocina, A. Vitalis, A. Caflisch, Sapphire-based clustering, J. Chem. Theor. Comp. 16 (10) (2020) 6383–6396.
[36] P.K. Baral, M. Swayampakula, M.K. Rout, N.N. Kav, L. Spyracopoulos, A. Aguzzi, M.N. James, Structural basis of prion inhibition by phenothiazine compounds, Structure 22 (2) (2014) 291–303.
[37] R. Chiesa, The elusive role of the prion protein and the mechanism of toxicity in prion disease, PLoS Path. 11 (2015) 1–7.
[38] L. Westergard, H. Lamb, D. Harris, The cellular prion protein (prp): its physiological function and role in disease, Biochim. et Biophys. Acta - Mol. Basis Dis. 1772 (2007) 629–644.
[39] J.A. Moreno, H. Radford, D.A. Barrett, P. Tsaytler, A. Bertolotti, A.E. Willis, M. Bushell, G.R. Mallucci, D. Peretti, J.R. Steinert, N. Verity, M. Guerra Martin, M. Halliday, J. Morgan, D. Dinsdale, C.A. Ortori, Sustained translational repression by eif2α—p mediates prion neurodegeneration, Nature 485 (7399) (2012) 507–511.
[40] P. Dametto, A.K.K. Lakkaraju, C. Bridel, L. Villiger, T. O'Connor, U.S. Herrmann, P. Pelczar, T. Rulicke, D. McHugh, A. Adili, A. Aguzzi, Neurodegeneration and

unfolded-protein response in mice expressing a membrane-tethered flexible tail of prp, PLoS One 10 (2015) 1–22.
[41] M. Beland, X. Roucou, The prion protein unstructured n-terminal region is a broad-spectrum molecular sensor with diverse and contrasting potential functions, J. Neurochem. 120 (6) (2012) 853–868.
[42] B. Wu, A.J. McDonald, K. Markham, C.B. Rich, K.P. McHugh, J. Tatzelt, D. W. Colby, G.L. Millhauser, D.A. Harris, The n-terminus of the prion protein is a toxic effector regulated by the c-terminus, eLife 6 (2017), e23473.
[43] K. Frontzek, Protective and Toxic Antibodies in Prion Diseases, Ph.D. thesis, University of Zurich, 2017, https://doi.org/10.5167/uzh-144021.
[44] J. Falsig, T. Sonati, U.S. Herrmann, D. Saban, B. Li, K. Arroyo, B. Ballmer, P. P. Liberski, A. Aguzzi, Prion pathogenesis is faithfully reproduced in cerebellar organotypic slice cultures, PLoS Pathog. 8 (2012) 1–13.